Classification: Physical Sciences – Chemistry

The origin of radiation tolerance in amorphous $Ge_2Sb_2Te_5$ phase-change random-access memory material

Konstantinos Konstantinou[a,1], Tae Hoon Lee[a], Felix C. Mocanu[a], and Stephen R. Elliott[a]

[a] Department of Chemistry, University of Cambridge, Lensfield Road, Cambridge CB2 1EW, UK.

[1] To whom correspondence may be addressed. E-mail: kk614@cam.ac.uk

Keywords: radiation damage, ion irradiation, phase-change memory, molecular dynamics, thermal spike

Abstract

The radiation-hardness of amorphous $Ge_2Sb_2Te_5$ phase-change random-access memory material has been elucidated by *ab initio* molecular-dynamics simulations. Ionising radiation events have been modelled in order to investigate their effect on the atomic and electronic structure of the glass. Investigation of the short- and medium-range order highlights a structural recovery of the amorphous network after exposure to the high-energy events modelled in this study. Analysis of the modelled glasses reveals specific structural rearrangements in the local atomic geometry of the glass, as well as an increase in the formation of large shortest-path rings. The electronic structure of the modelled system is not significantly affected by the ionising radiation events, since negligible differences have been observed before and after irradiation. These results provide a detailed insight into the atomistic structure of amorphous $Ge_2Sb_2Te_5$ after irradiation and demonstrate the radiation-hardness of the glass matrix.

Significance Statement

Radiation-hard non-volatile memories are in high demand by the space community for implementation in solid-state data recorders. In phase-change memories, binary data are represented as changes in structural phase rather than by stored electrical charge; thus, these devices are supposed to be tolerant to ionising radiation effects. In addition, they feature high cycling capability and large scaling potential. We present the first *ab initio* calculations of radiation-damage in amorphous phase-change materials. The glass shows a recovery from the damage imposed during ion irradiation, as it manages to maintain its amorphous network. Our simulations manifest the remarkable ability of $Ge_2Sb_2Te_5$ phase-change random-access memory material to be radiation-tolerant, and hence indicating its potential applications in future space and other radiation-present environments.

\body

Introduction

Radiation-hard non-volatile memories with large capacity, low production cost and small power consumption are in high demand by the space community for implementation in solid-state data recorders or as boot memories for microprocessors and field programmable gate arrays (1, 2). Floating-gate Flash memories have been able to be down-scaled for the past decades and have become the prevailing non-volatile memory technology. However, projecting into the next decade, the size down-scaling of floating-gate memory cells is becoming increasingly arduous and this corresponds to the most crucial obstacle to their use for devices in space (1). In a Flash memory, electrons are transferred from the floating gate to the substrate by tunnelling through a thin silicon dioxide (SiO_2) layer. A further thinning of the tunnelling oxide layer, which currently is about 5-10 nm, could result in an unsatisfactory reduction of the data-retention capability due to oxide leakage current, as well as other reliability issues (3). Thus, it is not very obvious how the floating-gate concept can be pushed much beyond the 20nm technology node, where a smaller tunnel oxide thickness is mandatory to keep the short channel effects under control.

Consequently, alternative storage concepts, which rely on completely different physical phenomena, are being actively developed by major semiconductor manufacturers. Phase-change random-access memory (PCRAM) technology is one of the most promising candidates to emerge for next-generation non-volatile memories, featuring high cycling capability, good data-retention characteristics, improved performance compared to Flash, as well as scalability down to the deca-nanometer range (4,5). In PCRAM, data storage is based on the structural phase of chalcogenide materials, which can be reversibly switched between amorphous and crystalline states by the application of suitable electrical pulses. The prototypical material employed in PCRAM is the ternary chalcogenide alloy, $Ge_2Sb_2Te_5$ (225GST), which, in the amorphous phase, features a high electrical resistance while the crystalline state is characterized by a low-resistance value. Hence, by measuring the 225GST resistance, it is possible to recover the stored information. 225GST is able to undergo fast and

reversible transitions between amorphous and crystalline phases upon Joule heating via voltage pulses (6). It also exhibits an appreciable electrical-resistivity contrast between amorphous and crystalline phases, a relatively stable amorphous phase and good data-storage lifetime characteristics (6).

Because floating-gate memory devices use trapped electrons to store information, they are susceptible to data corruption from radiation. On the contrary, in PCRAM, binary data are represented as a structural phase rather than by stored electrical charge; thus, it was presumed that these devices can be potentially tolerant to ionising radiation effects (3, 7). Radiation-hard memories of relatively small size (as compared to commercial devices), with 250-nm feature size, are already available (8). BAE systems has been developing a 4-Mbit non-volatile chalcogenide random-access memory, which is radiation-hard and meets rigorous reliability requirements, making it a promising candidate for spaceship applications (8).

Radiation effects on phase-change memories have been addressed by a few experimental studies (2, 3, 5, 8–11). A phase-change memory-cell array with a conventional 225GST film used as a storage medium has been fabricated by a standard complementary metal–oxide–semiconductor (CMOS) process (12). X-ray radiation experiments showed that both the higher and lower resistance states can be maintained, even at large radiation doses, highlighting an overall good radiation-tolerance ability (12). Total ionizing dose effects and single-event effects on a 64-kbit phase-change memory array integrated with radiation-hardened CMOS technology have showed a high resistance of the cell array against ionizing radiation (10). Irradiation of 180-nm cells, both with heavy ions and protons, confirmed their good response to radiation events, while the (small) observed degradation was attributed to radiation effects in selection devices and peripheral elements (5). Investigation of single-event effects on 90-nm phase-change memory cells in a large array (128-kbit) verified the radiation-hardness of the cells also for large-size memories (2).

The structural evolution of irradiated amorphous as-deposited 225GST films has been investigated experimentally by Raman spectroscopy (13). 225GST films were irradiated at

room temperature by 120 keV Sb^+ ions, and the Raman spectra were collected using a backscattering geometry. The Raman spectrum features two well-separated bands in the frequency range of 100–250 cm^{-1}. The intensity and the amplitude of the second peak, at approximately 152 cm^{-1}, were ascribed to an increase of homopolar bonds in the glass structure with an atomic configuration involving edge-sharing $GeTe_4$ tetrahedra (i.e. with distorted four-fold rings) (13).

In spite of such experimental studies, no atomistic calculations of ion irradiation in amorphous 225GST have been performed so far to investigate the radiation effects and shed light on the atomistic structure of the irradiated glasses. In this work, *ab initio* molecular-dynamics simulations were performed in order to examine the effect of ionising radiation on the atomic and electronic structures of amorphous 225GST. The observed structural motifs of the short- and medium-range order in our simulated glass structures allow us to gain direct insight into the structural evolution and the overall response of the material to radiation. In addition, the electronic-structure calculations provide further information about the effect of the radiation events on the electronic properties of the glass.

Results and Discussion

Radiation-damage cascades. Ion irradiation was modelled by carrying out a thermal-spike simulation (14, 15). The damage was inflicted on the amorphous network by a sudden transfer of kinetic energy from a highly energetic atom to another atom or a group of atoms that happen to suffer a collision. A Te atom was given an initial velocity consistent with kinetic energies of 50 eV, 100 eV or 200 eV, along a specific direction, to initiate a cascade event. The rest of the atoms were assigned a velocity distribution corresponding to a temperature of 300 K. These conditions are thus intended to mimic a radiation-damage event at 300 K, with the Te atom representing the primary knock-on atom (PKA). The system was then allowed to evolve and a stochastic-boundary-conditions approach was implemented in order to model the non-equilibrium dynamics of the radiation-damage cascade (see **Materials and Methods**, as well as the *SI Appendix*, for details).

The launch of the thermal spike raises the temperature of the modelled 225GST system initially to around 5200 K, 2750 K and 1520 K for the 200 eV, 100 eV and 50 eV initial PKA energies, respectively, revealing partial local melting of the glass structure. However, the average temperature of the modelled system exhibits an exponential reduction over time, as shown in **Fig. S2** in the *SI appendix*, which highlights the rapid dissipation of heat as the cascade evolves within the glass network. The average temperature remains above the melting point of 225GST, which is approximately 900 K, for 0.28 ps, 0.91 ps and 1.71 ps for the 50 eV, 100 eV and 200 eV PKA energies, respectively. It can be noted that this observation reflects the short lifetime of the ion-irradiation cascade within the host glass matrix for the simulated energies in this study and also the role of the Langevin-thermostat-coupled area around the simulation box, which is acting as a heat-sink, removing incident energy as it is dissipated through the material (16).

The PKA, after its detonation, travels through the glass network transferring large amounts of momentum and energy to the atoms along its path within the structure. Subsequently, these recipients of momentum get knocked from their positions and, in turn, also start moving like projectiles, thus creating an ion-irradiation cascade, shown in **Fig. 1*A*** for the 200 eV PKA thermal-spike energy. The colored lines highlight the trajectory of the atoms mostly involved in the cascade during the first 0.5 ps of the simulation, providing a sense of the evolution and spatial extent of the radiation-damage cascade. It can be noted that any deviation of the trajectory line, seen for the PKA atom for example, corresponds to a collision with another atom within the glass network and results in a significant reduction of its kinetic energy. It can be seen that the knock-on atoms, which gained enough energy from the impact with the PKA, were able to initiate sub-cascades within the glass structure. Thus, one of the prominent features in **Fig. 1*A*** is the fractal-like branching structure of the moving-atom trajectories, which arises from the highly energetic collisions involving the PKA and the subsequently displaced atoms in the glass structure. During these 500 fs of the simulated cascade, the damage imposed by the thermal-spike is most significant at approximately 350 fs, at which the formation of quite large voids is observed, as shown in **Fig. 1*B*** and discussed later.

Short-range order. Structural analysis of the short-range ordering has been performed in order to investigate the impact of the radiation-damage cascade on the glass network. The local structural environment in the irradiated glass samples was analyzed through the total radial distribution function (RDF), shown in **Fig. 2*A*** for the three thermal-spike PKA energies modelled in this work. The black dotted line corresponds to the total RDF of the amorphous 225GST model before irradiation. It can be observed that the final equilibrated structure shows, for every PKA energy, a recovery from the damage induced by the PKA and the subsequent cascades during the first few picoseconds of the simulation. The temporal evolution of the RDF along the molecular-dynamics trajectory, calculated for the 200 eV ion-irradiation simulation and presented in **Fig. S3** in the *SI appendix*, highlights the partial local melting of the glass structure due to the radiation-damage cascade and further confirms the recovery of the short-range order of the irradiated amorphous 225GST network. Moreover, the time evolution of the total number of bonds within the glass structure, shown in **Fig. 2*B***, verifies also this behavior. Despite the initially strong fluctuations of the number of bonds (formation and breakage of bonds during the cascade), the total proportion of bonds in the final equilibrated structures at 300 K is similar to that before the irradiation events for every PKA energy. It is noted that, throughout the simulation, we consider bond formation between two nearby atoms as long as the interatomic distance between these two atoms is shorter than or equal to 3.2 Å.

The average coordination numbers (CNs) around Ge, Sb and Te atoms in the final equilibrated irradiated model for the 200 eV thermal-spike simulation, calculated from the partial radial distribution functions, were found to be 4.1, 3.5 and 2.8 for Ge, Sb and Te, respectively, while in the glass before the ion-irradiation, they were 4.2, 3.7 and 2.9, respectively for the same type of atoms. Hence, this comparison reveals that the coordination environments of the atomic species in the amorphous structure are almost unaffected by the radiation-damage cascade, since only a slight reduction of the CNs in the simulated model was observed, indicating that the glass structure is able to recover after the ion-irradiation cascade and becomes only marginally under-coordinated. This behavior suggests that 225GST exhibits an

overall good structural recovery after exposure to the high-energy events modelled in this study, since it manages to maintain its amorphous structure – i.e. it is radiation-hard.

The time evolution of the calculated proportion of homopolar and so-called “wrong” bonds (Ge–Ge, Ge–Sb, Sb–Sb and Te–Te) in the simulated models, shown in **Fig. 3*A***, reveals an increase of such “wrong” bonds in the glass structure after the radiation-damage cascades, which is indicative of the specific structural rearrangements that occurred within the glass network. The 200 eV PKA cascade leads to a three times higher total number of homopolar bonds in the glass structure, while there is a systematic increase in the “wrong” bonds with respect to the thermal-spike energy. The edge- to corner-sharing $GeTe_4$ tetrahedron ratio was also quantified for the irradiated glass samples and is plotted in **Fig. 3*B***. An increased proportion of edge-sharing $GeTe_4$ tetrahedra with increasing PKA energy was observed, which is in accordance with the calculated trend for the increasing proportion of “wrong” bonds within the glass structure of the irradiated 225GST samples. Moreover, it can be noted that these simulation results agree well with the experimental study of De Bastiani *et al*. (13), in which the observed Raman-spectra peaks were attributed to the induced formation of homopolar bonds and to an increased proportion of $GeTe_4$ edge-sharing tetrahedra in the irradiated amorphous structure.

Medium-range order. The effect of the radiation-damage cascade on the medium-range order of the amorphous network was characterized through the ring-size distribution and an atomic-vacancy analysis. The distribution of shortest-path rings, presented in **Fig. 4*A*** for the 200 eV thermal-spike simulation, was calculated using the Franzblau algorithm (17) with a bonding cutoff distance of 3.2 Å. Before the ion-irradiation, the glass model shows the usual patterns reported in the literature for the amorphous structure of 225GST (18, 19). Four-fold rings are the most dominant rings within the glass network, while the large proportion of even-membered rings (4-, 6-, 8- and 12-fold rings) highlights the preference for ABAB bond alternation (A = Ge, Sb; B = Te). At approximately 300 fs after the detonation of the thermal-spike, the ion-irradiation cascade has produced the most significant damage in the glass

structure (see **Fig. 1*B***) and a calculation of the ring-size distribution reveals a considerable increase in the number of 3-, 6- and 7-fold rings. Nevertheless, in the final equilibrated structure at 300 K, the amount of 3-fold rings is reduced back to its initial value. A comparison with the ring-size distribution of liquid 225GST, calculated from a model which was generated at 1200K with *ab initio* molecular-dynamics simulations (20), suggests that the final irradiated structure is somewhat more “liquid-like” than the initial amorphous 225GST model, since an almost uniform distribution of 8-, 9-, 10-, and 11-fold rings is revealed (see **Fig. S4** in the *SI appendix* for the statistics of shortest-path rings in the liquid phase of 225GST). The ring-size distribution in the final equilibrated structure also shows an increase in the formation of large shortest-path rings, i.e. 12-, 13-, 14- and 15-fold rings, within the glass network, which were probably formed during the fast thermal quench of the simulated cascade.

Vacancies and voids are typically formed within the structure of amorphous 225GST and play an important role in the atomic dynamics of the material (21). The time evolution of the volume of the vacancies, calculated using a Voronoi-tesselation analysis, for the 200 eV thermal-spike simulation is shown in **Fig. *4B***. The vacancy distribution before irradiation and for the 200 eV ion-irradiation simulation at 300 fs, as well as for the subsequent final equilibrated structure at 300 K, are shown in **Fig. 4*C***. Based on the study of the vacancies, and as expected from the rest of the analysis so far, the radiation-damage cascade results in a significant increase in the formation of voids during the early stages of the simulation (at approximately 0.3 ps after the beginning of the simulation). In addition, the large volume of the generated vacancies within the amorphous network of the simulated structure is highlighted in the inset to **Fig. 4*C***. However, the large vacant sites (with volume > 40 $Å^3$) survived only for less than 1 ps inside the glass network (see **Fig. S5** in the *SI appendix*). Hence, in the final equilibrated structure, these large voids have disappeared, revealing a partial recovery of the medium-range order of the glass network, i.e. a net tolerance to radiation.

The temporal evolution of the number of atoms lying in planes, shown in **Fig. 5** for the 200 eV ion-irradiation simulation, further validates the discussed pattern. A plane consists of at least two four-fold rings connected in parallel, i.e. with a bond angle of 180° ± 20° (22). The total

number of atoms involved in forming planes was calculated at each time-step along the molecular-dynamics trajectory and is shown in the bottom panel of **Fig. 5**. The size of a plane, which can be defined as the number of four-fold rings forming the plane, shows a certain distribution and varies significantly during the radiation-damage cascade, as also highlighted in the top panel of **Fig. 5** for three selected atomic configurations during the ion-irradiation simulation.

An overall loss of the quasi-binary chemical order was observed at 0.3 ps, indicating a dramatic modification of the medium-range order at the maximum-damage point of the simulated cascade. However, the proportion of atoms in planes in the final equilibrated irradiated 225GST model is almost the same as that of the initial glass structure before irradiation, further confirming the recovery of the glass network after exposure to an ion-irradiation event and demonstrating its radiation hardness.

Electronic structure. The calculated electronic structure of the amorphous 225GST model before the irradiation events shows a HOMO-LUMO Kohn-Sham band gap of 0.66 eV for the relaxed ground state, which agrees very well with the experimentally reported values (ranging between 0.6 and 0.8 eV) (23, 24), as well as with previous modelling studies (25, 26). After equilibration of each simulated radiation-damage cascade, the irradiated glass samples were cooled down to 0 K and their electronic structure was calculated in order to examine the effect of the ionizing radiation on the electronic properties of the amorphous structure. Band gaps of 0.61 eV, 0.72 eV and 0.62 eV were obtained for the 50 eV, 100 eV and 200 eV thermal-spike PKA energies, respectively, indicating that the absolute value of the band gap was not significantly affected by the ion-irradiation, which remained within the range of the experimental values for every irradiated glass model. In addition, the total density of states (DOS) for the 200 eV thermal-spike simulation is shown in **Fig. 6*A***, in comparison with the density of states of the initial 225GST model, and highlights the negligible differences in the electronic structure of the glass before and after irradiation (see **Fig. S6** in the *SI appendix* for the partial electronic densities of states of the two glass models).

The evolution of the electronic structure was also analyzed for the 200 eV ion-irradiation simulation and is shown in **Fig. 6*B***. During the radiation-damage cascade, defect states arise in the electronic structure of the glass, which are related to the impact of the cascade on the amorphous network. In addition, the band gap of the modelled system shows some fluctuations along the molecular-dynamics trajectory. However, these defects disappear during the quench of the cascade and the electronic structure exhibits a remarkable healing and reversibility. In the final equilibrated irradiated structure, there are no defect states left and the band gap reverts to a value (0.64 eV) similar to that before irradiation (0.66 eV), highlighting the ability of amorphous 225GST to be radiation-tolerant.

A more detailed inspection of the band edges reveals some differences between the irradiated sample and the glass model before the thermal-spike simulation. The visualisation of the bottom of the conduction band through the lowest unoccupied molecular orbital (LUMO) of the simulated glass structure before irradiation, shown in **Fig. S7*A*,** and after irradiation, shown in **Fig. S7*B***, highlights the distinct differences in the nature of electron localisation within the glass network for the state which describes the bottom of the conduction band. Before ion-irradiation, the LUMO state of the 225GST model is mainly localised on Te atoms, which are members of $GeTe_4$ tetrahedral units within the glass network, whereas after the 200 eV thermal-spike simulation, the LUMO state of the irradiated glass sample has preferential localisation on Ge and Sb atoms, which form small clusters in the glass structure.

Conclusions

The local environments of ion-irradiated amorphous 225GST have been investigated for the first time by means of *ab initio* molecular-dynamics simulations employing a stochastic boundary-condition approach. Atomistic simulations are able to provide local atomic pictures of the glass structure and a detailed insight into the response of the amorphous 225GST network to ionizing-radiation events, demonstrating the remarkable ability of 225GST phase-change random-access memory material to be radiation-tolerant, and hence indicating its potential applications in future space and other radiation-present environments.

The appreciable void volume present in amorphous 225GST may be considered responsible for the origin of radiation-tolerance of the material. During the radiation-damage cascade, the breakage of atomic bonds due to collisions inside the glass structure results in the formation of large voids (with a large volume, as highlighted in the medium-range order analysis) within the amorphous network. As the cascade evolves, the density at the surface of these cavities increases and hence reformation of the bonds is intitiated, leading to the generation of large ring structures. These large shortest-path rings act possibly as scaffolds for the recovery of the amorphous structure, whille some of them remain within the glass network at the final equilibrated simulated structure. Consequently, the densification at the boundary of large cavities generated during the initial stages of the ion-irradiation, followed by rarefaction, local relaxation and reordering within the glass structure during the natural quench of the radiation-damage cascade, seems to be the driving force for the recovery of the chemical and topological order of amorphous 225GST.

Moreover, in amorphous 225GST, compared to other materials, there are a large number of different local environments with various coordinations and degrees of ordering which can co-exist inside the glass. This indicates that 225GST has a highly flexible structure induced by the existence of weak chemical bonds and lone-pairs (20). Thus, the diversity of bonding environments present in the material is likely to lower the energy barrier for structural reconfiguration, thereby accelerating the bond reformation and thus facilitating the recovery process of the amorphous network. In this respect, based on our data and the specific characteristics of 225GST, we assume that a fast recovery after irradiation is likely to be observed in amorphous materials which feature a similar nature of highly-flexible chemical bonding, and/or an ample vacancy volume within the glass network.

Based on our modelling results, an increased proportion of edge-sharing $GeTe_4$ tetrahedra was observed inside the glass structure after exposure to ion-irradiation, which was correlated with the induced number of homopolar bonds found in the final equilibrated structure. A connection between edge-sharing polyhedral connectivity and “fragility“ has been highlighted in previous experimental and theoretical studies for other amorphous chalcogenide systems

(27, 28). Hence, our radiation-damage simulations reveal specific structural modifications of the medium-range order during the recovery process that have been previously linked to the important aspect of fragility of phase-change materials (i.e. the fact that the viscosity of the liquid behaves in a markedly non-Arrhenius fashion), which, in turn, is correlated to the rapid crystallization of the materials. Consequently, such an understanding of how ion-irradiation affects the chemical bonding during the recovery process within the glass network is invaluable in the design of phase-change materials with controlled crystallization rate and fragility.

The crystalline phase of 225GST might exhibit a similar radiation-tolerance up to some energy threshold, beyond which amorphization might be expected to become irreversible (metamict behavior). The cubic crystalline phase of 225GST, mainly involved in PCRAM applications, is metastable, disordered and has intrinsic vacant sites (~10%). However, generating an initial cubic crystalline structure as a candidate for radiation-damage simulations is challenging in itself. In addition, such an investigation would require a large number of simulations exploring systematically different initial energies for the primary knock-on atom for each crystalline model, as well as different atomic species and firing directions inside the computational cell. The isotropic nature of the glass makes it less sensitive to the firing direction of the primary knock-on atom and hence to the initiation of the radiation-damage cascade inside the model.

It should be noted that high-energy radiation events in ionic and covalent materials can lead to highly excited electronic configurations (29). Cascade simulations can provide a solid understanding of the fundamental mechanisms involved in radiation damage; however, they are restricted to modelling radiation events that transfer energy solely to the nuclei since they neglect the effects of excited electrons. In this work, it has been implicitly assumed that, for a relatively low energy of the primary knock-on atom, the dynamics of the collisions inside the glass are electronically adiabatic and that ground-state density-functional theory, coupled with molecular-dynamics, provides a sufficient picture for the effects of the radiation-damage cascade in the amorphous network of the glass model. We also note that, due to the relatively small size of the glass model and the low initial thermal-spike kinetic energy, the amount of

data generated in this study might be insufficient for an accurate statistical representation of the influence of the radiation-damage cascade on the amorphous network. Nevertheless, our results are sufficient in order to be able to characterize qualitatively the types of local structures before and after ion irradiation and to demonstrate the nature of radiation tolerance in this material.

Materials and Methods

Modelled system. A 315-atom structural model of amorphous 225GST, generated by *ab initio* molecular-dynamics simulation in a previous work of our group (20), was used to model radiation damage in this study, with the individual number of atoms being Ge = 70, Sb = 70 and Te = 175, while the simulation cell size corresponds to the experimental density (5.88 g/cm^3) (30).

Radiation-damage modelling and first-principles molecular-dynamics simulations. Ion irradiation was modelled by performing thermal-spike simulations (14,15). The scheme of mixed NVE Born-Oppenheimer and NVT Langevin *ab initio* molecular dynamics (31, 32), as implemented in the CP2K code (33), was applied in the simulations performed in this work (see *SI Appendix* for details). A schematic diagram of the simulation set-up is shown in **Fig. S1** in the *SI Appendix*. A Te primary-knock-on atom (PKA) was given an initial velocity corresponding to kinetic energies of 50 eV, 100 eV or 200 eV, and the cascade was launched from one corner along the body diagonal of the computational cell to maximize the range. The rest of the atoms were assigned a velocity distribution corresponding to a temperature of 300K. The system was then allowed to evolve undergoing NVE Born-Oppenheimer *ab initio* molecular dynamics. A damping outer layer of 1.0 Å thickness was placed around the edges of the periodic directions of the 21.65 Å simulation box in order to model the dissipation of heat from the irradiated area by using generalized Langevin molecular dynamics, i.e. to dampen thermal motion as it reaches the edges, and hence to avoid the diverging cascade of damage from bouncing back from the boundary (34). Hence, the velocities of a selection of

atoms around the boundary perimeter were stochastically scaled and kept at 300 K at every molecular-dynamics step (16).

The total simulation time of the ion irradiation was 12-16 ps, depending on the respective chosen thermal-spike energy, which was sufficient for the system to equilibrate at 300 K. A variable time-step approach was followed for the integration of the equations of motion during the simulations. A time-step of 0.25 fs was used for the first 2-4 ps of each radiation-damage cascade, following by one of 0.5 fs for the period 5-7 ps and finishing with a time-step of 1 fs for the last 5 ps of each trajectory.

Electronic-structure calculations. After the equilibration of the radiation-damage cascades, the glass structures were cooled down to 0 K with a quenching rate of -15 K/ps in order to model the electronic structure of the irradiated samples. The atomic geometry of each glass model was optimized, and the electronic structure was calculated by using the non-local functional PBE0 with a cutoff radius of 3 Å for the truncated Coulomb operator (35). It is noted that the computational cost of hybrid-functional calculations can be reduced by using the auxiliary density-matrix method (ADMM) (36), as employed in previous modelling studies of amorphous materials (37, 38). The Broyden–Fletcher–Goldfarb–Shanno (BFGS) algorithm was applied in the geometry optimizations, and the forces on atoms were minimized to within 40 pN (2.5×10^{-2} eV Å^{-1}). In order to investigate the evolution of the electronic structure, six configurations along the molecular-dynamics trajectory for the 200eV ion-irradiation simulation were selected (at 350fs, 1ps, 2ps, 5ps, 10ps and 16ps) and the electronic structure was calculated by performing geometry optimization, for each of them, with the same hybrid functional as above.

Acknowledgements

This work was supported by the UK Engineering and Physical Sciences (EPSRC) grant, EP/N022009 ("Development and Application of Non-Equilibrium Doping of Amorphous Chalcogenides"). F.C.M. would like to acknowledge the EPSRC Centre for Doctoral Training in Computational Methods for Materials Science for funding under grant number EP/L015552/1. *Via* our membership of the UK's HEC Materials Chemistry Consortium, which is funded by EPSRC (EP/L000202), this work used the ARCHER UK National Supercomputing Service (http://www.archer.ac.uk). K.K. acknowledges the use of the UCL Grace High Performance Computing Facility (Grace@UCL), and associated support services, in the completion of this work.

Author contributions

K.K. designed the study and the concept was developed by all authors. K.K. performed all the simulations. K.K., T.H.L. and F.C.M. analyzed the simulation results and constructed the figures. K.K. and S.R.E. wrote the manuscript and all authors commented on the paper.

References

1. Gerardin S, Paccagnella A (2010) Present and future non-volatile memories for space. *IEEE Trans On Nucl Sci* 57:3016–3039.
2. Gerardin S, Bagatin M, Paccagnella A, Visconti A, Bonanomi M, Pellizzer F, Vela M, Ferlet-Cavrois V (2011) Single event effects in 90-nm phase change memories. *IEEE Trans On Nucl Sci* 58:2755–2760.
3. Gasperin A, Wrachien N, Paccagnella A, Ottogalli F, Corda U, Fuochi PG, Lavalle M (2008) Total ionizing dose effects on 4 Mbit phase change memory arrays. *IEEE Trans On Nucl Sci* 55:2090–2097.
4. Bez R, Pirovano A (2004) Non-volatile memory technologies: emerging concepts and new materials. *Mat Science in Semic Proces* 7:349–355.
5. Pirovano A, Redaelli A, Pellizzer F, Ottogalli F, Tosi M, Ielmini D, Lacaita AL, Bez R (2004) Reliability study of phase-change nonvolatile memories. *IEEE Trans On Dev And Mat Reliab* 4:422.

6. Raoux S, Welnic W, Ielmini D (2010) Phase change materials and their application to nonvolatile memories. *Chem Rev* 110:240–267.
7. Ovshinsky SR, Evans EJ, Nelson DL, Fritzsche H (1968) Radiation hardness of ovonic devices. *IEEE Trans On Nucl Sci* 15:311–321.
8. Rodgers J, Maimon J, Storey T, Lee D, Graziano M, Rockett L, Hunt K (2008) A 4-Mb non-volatile chalcogenide random access memory designed for space applications: Project status update. Presented at Non-Volatile Memory Technology Symposium, Pacific Grove, CA.
9. Bernacki S, Hunt K, Tyson S, Hudgens S, Pashmakov B, Czubatyj W (2000) Total dose radiation response and high temperature imprint characteristics of chalcogenide based RAM resistor elements. *IEEE Trans On Nucl Sci* 47:2528–2533.
10. Maimon JD, Hunt K, Burcin L, Rodgers J (2003) Chalcogenide memory arrays: characterizartion and radiation effects. *IEEE Trans On Nucl Sci* 50:1878–1884.
11. Maimon JD, Hunt K, Rodgers J, Burcin L, Knowles K (2004) Results of radiation effects on a chalcogenide non-volatile memory array. *IEEE Aerospace Conf Proc* 4:2306–2315.
12. Wu L-C et al. (2006) Total dose radiation tolerance of phase change memory cell with GeSbTe alloy. *Chin Phys Lett* 23:2557.
13. De Bastiani R, Piro AM, Grimaldi MG, Rimini E, Baratta GA, Strazzulla G (2008) Ion irradiation-induced local structural changes in amorphous $Ge_2Sb_2Te_5$ thin film. *Appl Phys Lett* 92:241925.
14. Prasai K, Drabold DA (2014) Simulations of silver-doped germanium-selenide glasses and their response to radiation. *Nanoscale Res Lett* 9:594.
15. Kilymis DA, Delaye J-M, Ispas S (2016) Nanoindentation of the pristine and irradiated forms of a sodium borosilicate glass: Insights from molecular dynamics simulations. *J Chem Phys* 145**:**044505.
16. Dunn AR, Duffy DM (2011) A molecular dynamics study of diamond and graphite under tritium bombardment. *J Appl Phys* 110:104307.
17. Franzblau DS (1991) Computation of ring statistics for network models of solids. *Phys Rev B* 44:4925–4930.
18. Kohara S et al. (2006) Structural basis for the fast phase change of $Ge_2Sb_2Te_5$: Ring statistics analogy between the crystal and amorphous states. *Appl Phys Lett* 89:201910.
19. Akola J, Jones RO (2008) Density functional study of amorphous, liquid and crystalline $Ge_2Sb_2Te_5$: homopolar bonds and/or AB alternation? *J Phys: Condens Matter* 20: 465103.

20. Lee TH, Elliott SR (2017) The relation between chemical bonding and ultrafast crystal growth. *Adv Mater* 29:1700814.
21. Lee TH, Elliott SR (2011) Structural role of vacancies in the phase tranistion of $Ge_2Sb_2Te_5$ memory materials. *Phys Rev B* 84:094124.
22. Lee TH, Elliott SR (2011) *Ab Initio* computer simulation of the early stages of crystallization: application to $Ge_2Sb_2Te_5$ phase-change materials. *Phys Rev Lett* 107:145702.
23. Lee B-S et al. (2005) Investigation of the optical and electronic properties of $Ge_2Sb_2Te_5$ phase change material in its amorphous, cubic, and hexagonal phases. *J Appl Phys* 97:093509
24. Kato T, Tanaka K (2005) Electronic properties of amorphous and crystalline $Ge_2Sb_2Te_5$ films. *Jpn J Appl Phys* 44:7340.
25. Caravati S, Bernasconi M, Kühne TD, Krack M, Parrinello M (2009) First-principles study of crystalline and amorphous $Ge_2Sb_2Te_5$ and the effects of stoichiometric defects. *J Phys: Condens Matter* 21:255501.
26. Kozyukhin SA, Nguyena HP, Tsendin KD, Prikhodko OY (2016) Optical properties of amorphous thin films Ge-Sb-Te phase change materials. *Int J Adv Res in Phys Sci* 3:1–6.
27. Tatsumisago M, Halfpap BL, Green JL, Lindsay SM, Angell CA (1990) Fragility of Ge-As-Se glass-forming liquids in relation to rigidity percolation, and the Kauzmann paradox. *Phys Rev Lett* 64:1549.
28. Wilson M, Salmon PS (2009) Network topology and the fragility of tetrahedral glass-forming liquids. *Phys Rev Lett* 103:157801.
29. Duffy DM, Daraszewicz SL, Mulroue J (2012) Modelling the effects of electronic excitations in ionic-covalent materials. *Nucl Instrum and Meth in Phys Res B* 277:21.
30. Njoroge WK, Wöltgens HW, Wuttig M (2002) Density changes upon crystallization of $Ge_2Sb_{2.04}Te_{4.74}$ films. *J Vac Sci Technol* 20:230.
31. Kantorovich L, Rompotis N (2008) Generalized Langevin equation for solids. II. Stochastic boundary conditions for nonequilibrium molecular dynamics simulations. *Phys Rev B* 78:094305.
32. Ricci A, Ciccotti G (2003) Algorithms for Brownian dynamics. *Mol Phys* 101:1927–1931.
33. VandeVondele J, Krack M, Mohamed F, Parrinello M, Chassaing T, Hutter J (2005) QUICKSTEP: Fast and accurate density functional calculations using a mixed Gaussian and plane waves approach. *Comput Phys Commun* 167:103–128.
34. Åhlgren EH, Kotakoski J, Lehtinen O, Krasheninnikov AV (2012) Ion irradiation tolerance of graphene as studied by atomistic simulations. *Appl Phys Lett* 100:233108.

35. Guidon M, Hutter J, VandeVondele J (2009) Robust periodic Hartree-Fock exchange for large-scale simulations using Gaussian basis sets. *J Chem Theory Comput* 5: 3010–3021.
36. Guidon M, Hutter J, VandeVondele J (2010) Auxiliary density matrix methods for Hartree-Fock exchange calculations. *J Chem Theory Comput* 6:2348–2364.
37. El-Sayed AM, Watkins MB, Shluger AL, Afanas'ev, VV (2014) Nature of intrinsic and extrinsic electron trapping in SiO_2. *Phys Rev B* 89:125201.
38. Konstantinou K, Duffy DM, Shluger AL (2016) Structure and luminescence of intrinsic localized states in sodium silicate glasses. *Phys Rev B* 94:174202.

Figure Legends

Fig. 1. (A) Spatial evolution of the radiation-damage cascade in amorphous $Ge_2Sb_2Te_5$ for a 200eV thermal-spike Te atom during the first 500fs. Ge atoms are blue, Sb are red and Te are yellow. The Te PKA is represented as a large purple sphere. At the instant of closest approach, the velocities are transiently very small and the forces are enormous; the repulsion between the two atoms then splits the cascade and converts some of the potential energy into kinetic energy spread between the two atoms. The diffusion pathways of the PKA and the subsequent knocked-on atoms within the glass structure are highlighted by the respective colored line (purple for the PKA and black for the rest of the atoms). (B) The damage inflicted by the Te thermal-spike in the glass structure is most conspicuous at approximately 350fs after the detonation of the PKA, since relatively large voids are formed within the glass network at that time.

Fig. 2. (A) Total radial distribution functions for the final equilibrated irradiated amorphous 225GST models at 300K for the three different thermal-spike energies simulated in this work. The dashed line corresponds to the total RDF of the 225GST glass before irradiation. No significant differences can be observed in the amorphous structure before and after irradiation, indicating that 225GST is radiation-hard. (B) Temporal evolution of the total number of bonds within the glass structure calculated for each radiation-damage cascade. During the first few

picoseconds of the simulation, large fluctuations can be observed, highlighting the exposure of the structure to highly energetic collisions. Nevertheless, in the models equilibrated at 300 K, the total number of bonds is similar to that before irradiation (shown as the dashed line). A radial cut-off distance of 3.2 Å was used to specify bond formation in the simulated structures during the radiation-damage cascade.

Fig. 3. (A) Time evolution of the proportion of homopolar and so-called "wrong" bonds (Ge–Ge, Ge–Sb, Sb–Sb and Te–Te) in the glass structure for each ion-irradiation simulation. There is an increase in the population of homopolar bonds within the glass network in the final equilibrated ion-irradiated 225GST glass model, for each thermal-spike energy, with respect to the number of "wrong" bonds before irradiation (indicated with the dashed line). (B) Edge- to corner-sharing ratio of $GeTe_4$ tetrahedra in the glass structure calculated before and after irradiation for each PKA energy. There is a systematic reduction in the proportion of corner-sharing tetrahedra correlated with the increase of the homopolar bonds within the glass network. The dashed line is included as a guide for the eye.

Fig. 4. (A) Ring-size distribution in amorphous $Ge_2Sb_2Te_5$. The shortest-path rings were calculated in the glass structure before irradiation, for the 200eV radiation-damage cascade at 300 fs after the detonation of the thermal-spike, and for the final equilibrated structure at 300 K. The dominant topological unit throughout the simulation remains the 4-fold ring. The ion-irradiation cascade at 0.3 ps after the beginning of the event results in the generation of a large number of 3- and 6-fold rings, which then disappear during the subsequent thermal quench, while the final equilibrated structure contains a higher number of large rings (12-15 membered). (B) Time evolution of the volume of the vacancies, calculated using a Voronoi-tesselation analysis, for the 200eV thermal-spike simulation. (C) Vacancy distribution in the 225GST model before irradiation, at 300 fs in the 200eV ion-irradiation simulation and in the final equilibrated structure at 300 K. There is a significant increase in the size of the cavities formed within the glass network at 0.3 ps, while these larger voids have disappeared in the

final equilibrated structure. Inset: Volume of the vacancies (highlighted in green) at 300 fs generated due to the 200eV radiation-damage cascade in the glass structure.

Fig. 5. Time evolution of the number of atoms which belong to a plane within the glass network for the 200eV thermal-spike simulation. The medium-range order seems to be almost completely destroyed within the 225GST glass model during the first few picoseconds of the simulation, which is related to the damage caused by the ion-irradiation cascade in the amorphous network. However, the final equilibrated structure shows a recovery of the medium-range order, highlighting the radiation tolerance of 225GST in maintaining its amorphous structure after an irradiation event. Also shown are snapshots of the atomic configurations at three times during the simulation, as marked. Ge atoms are blue, Sb are red, and Te are yellow. The Te PKA is represented with a large yellow sphere, highlighted by the dashed white circle. Atoms in planes are marked in green. A plane consists of at least two four-fold rings connected in parallel (i.e. with a bond angle of 180° ± 20°). Four-fold rings are considered when four atoms form a planar square with a bond angle of 90° ± 20°.

Fig. 6. (A) Total electronic density of states of the amorphous 225GST model before irradiation and after the 200eV radiation-damage simulation. The obtained HOMO-LUMO band gap is 0.66eV and 0.62eV before and after irradiation, respectively, while no significant overall differences can be observed between the electronic structures of the two models. (B) Total electronic densities of states near the top of the valence band and the bottom of the conduction band for six configurations of the irradiated glass model, at different times, along the molecular-dynamics trajectory for the 200eV thermal-spike simulation. The time evolution of the electronic structure reveals the generation of defect states due to the damage imposed on the amorphous network from the cascade. A noticeable healing and reversibility of the electronic structure is highlighted towards the end of the ion-irradiation simulation, pointing out the ability of amorphous 225GST to be radiation-tolerant with respect to its electronic structure as well.

(A)

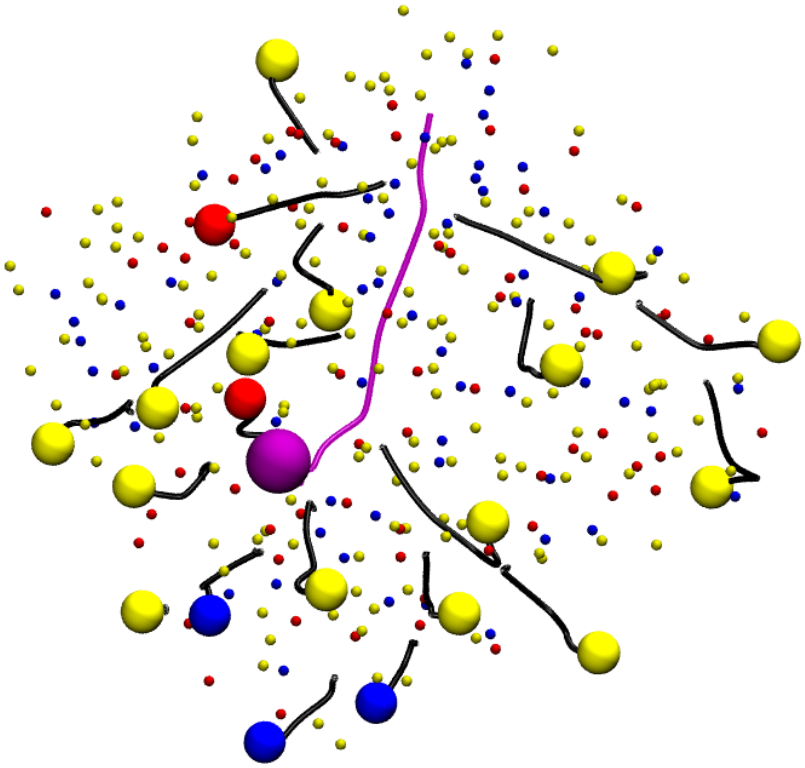

(B)

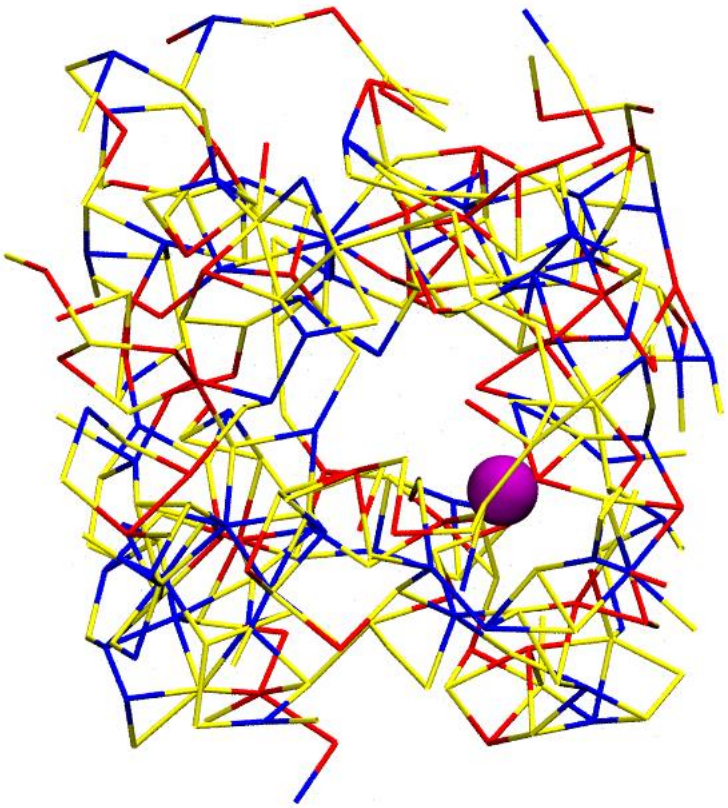

(A)

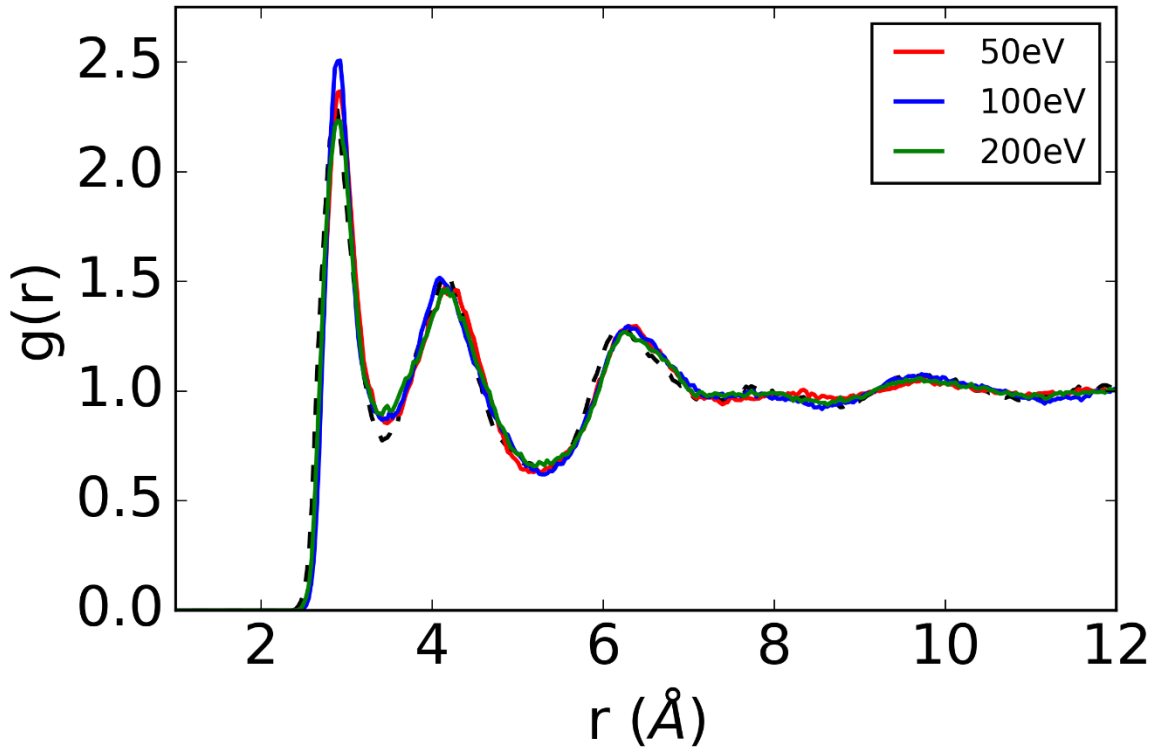
50eV
100eV
200eV
g(r)
r (Å)
0.0
0.5
1.0
1.5
2.0
2.5
2
4
6
8
10
12

(B)

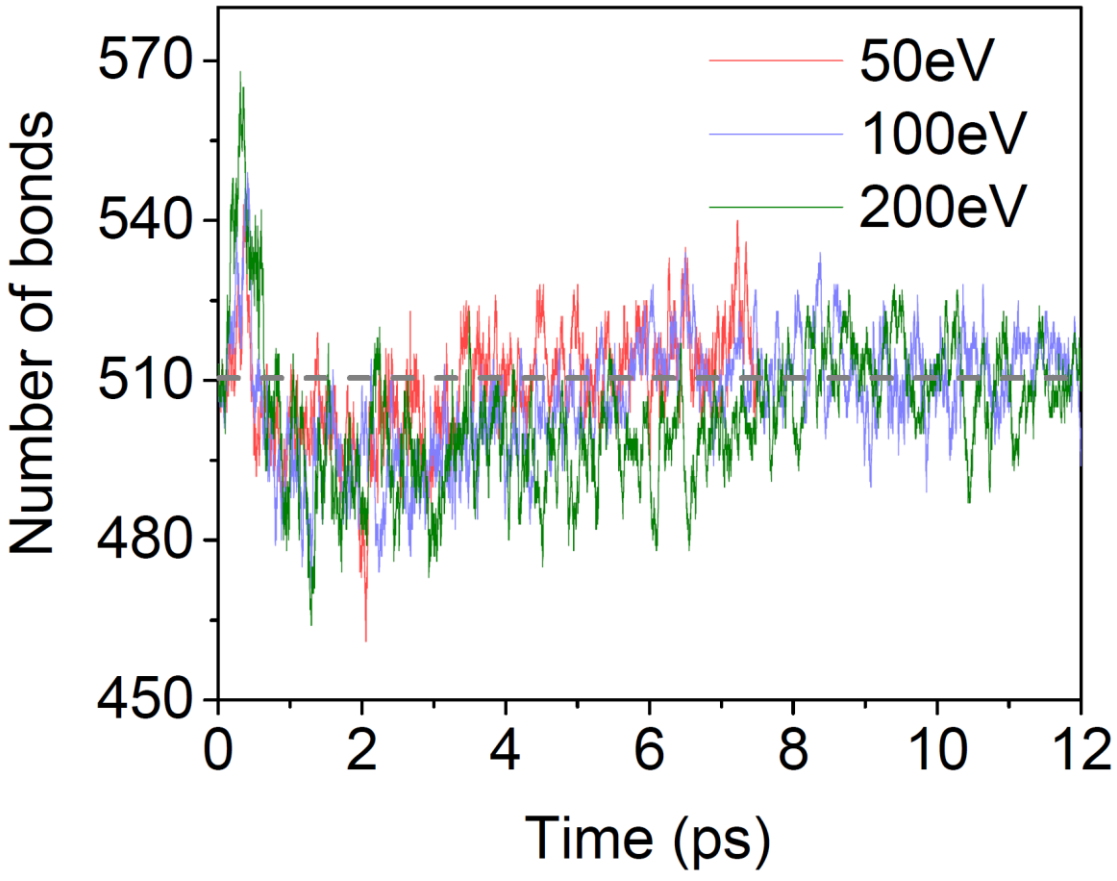
50eV
100eV
200eV
Number of bonds
Time (ps)
450
480
510
540
570
0
2
4
6
8
10
12

(A)

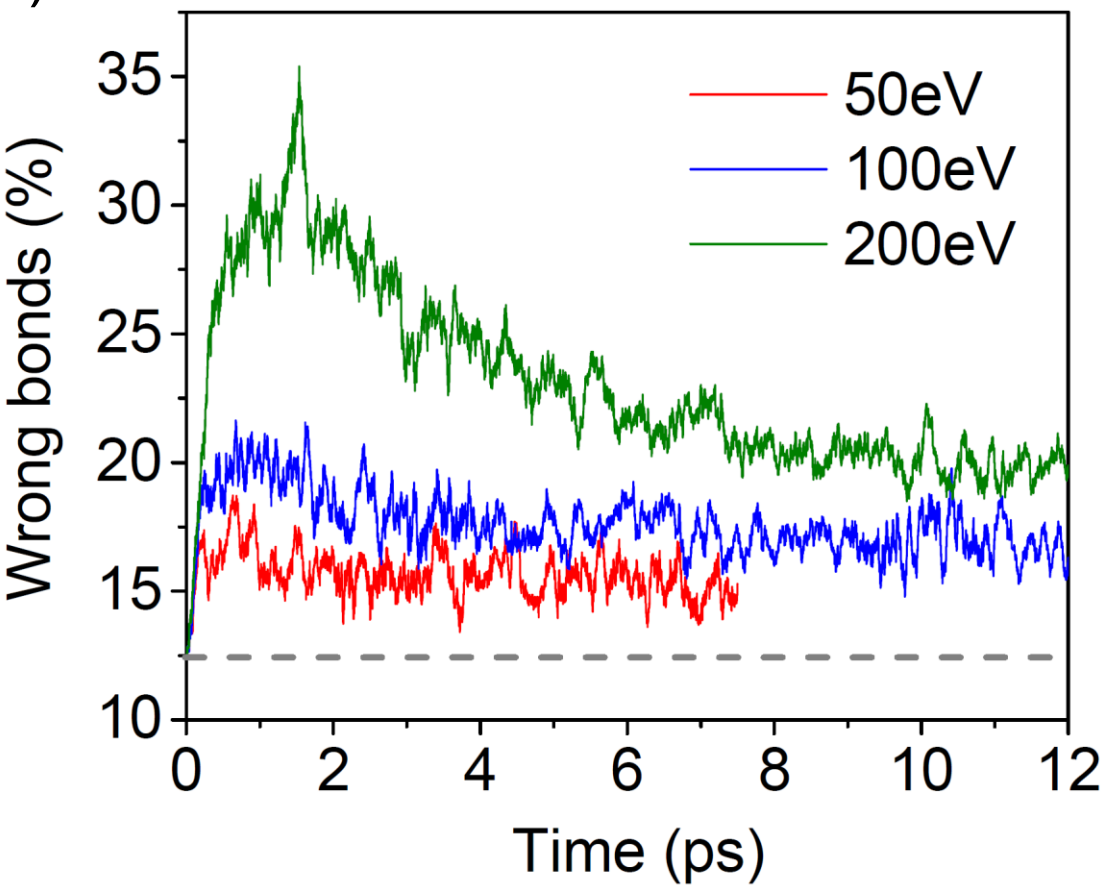
Wrong bonds (%)
35
30
25
20
15
10
0
2
4
6
8
10
12
Time (ps)
50eV
100eV
200eV

(B)

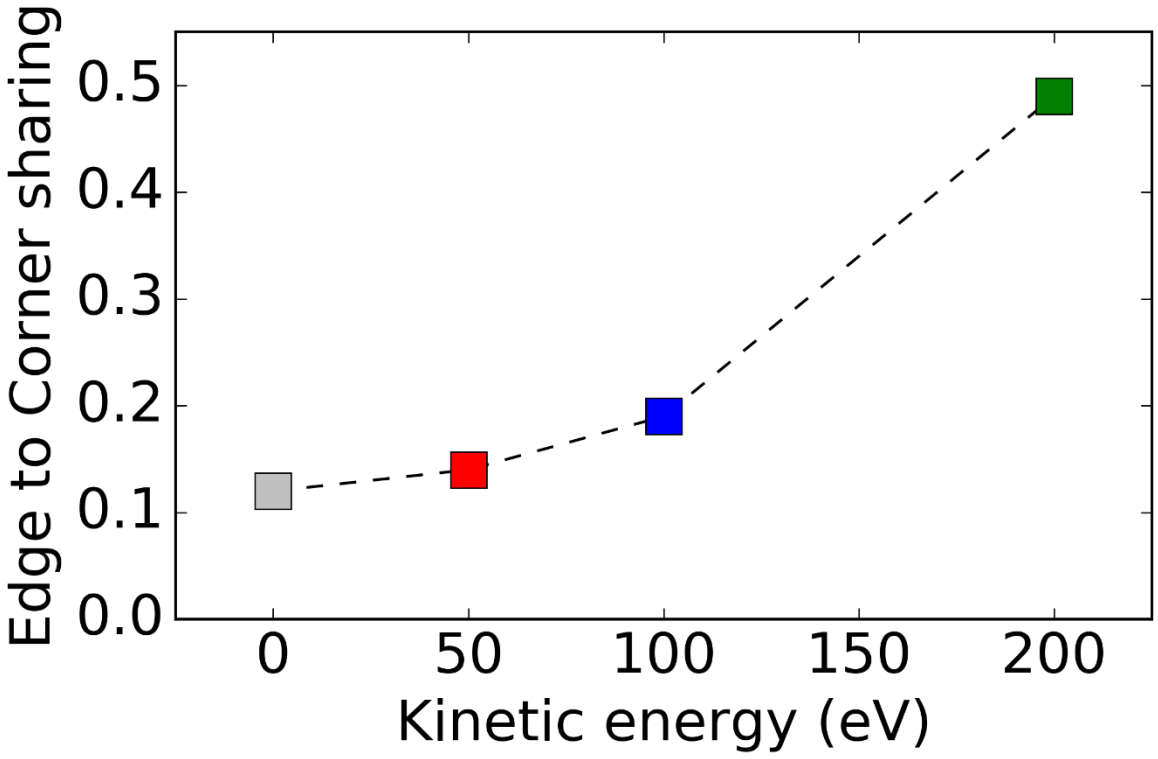
Edge to Corner sharing
0.5
0.4
0.3
0.2
0.1
0.0
0
50
100
150
200
Kinetic energy (eV)

(A)

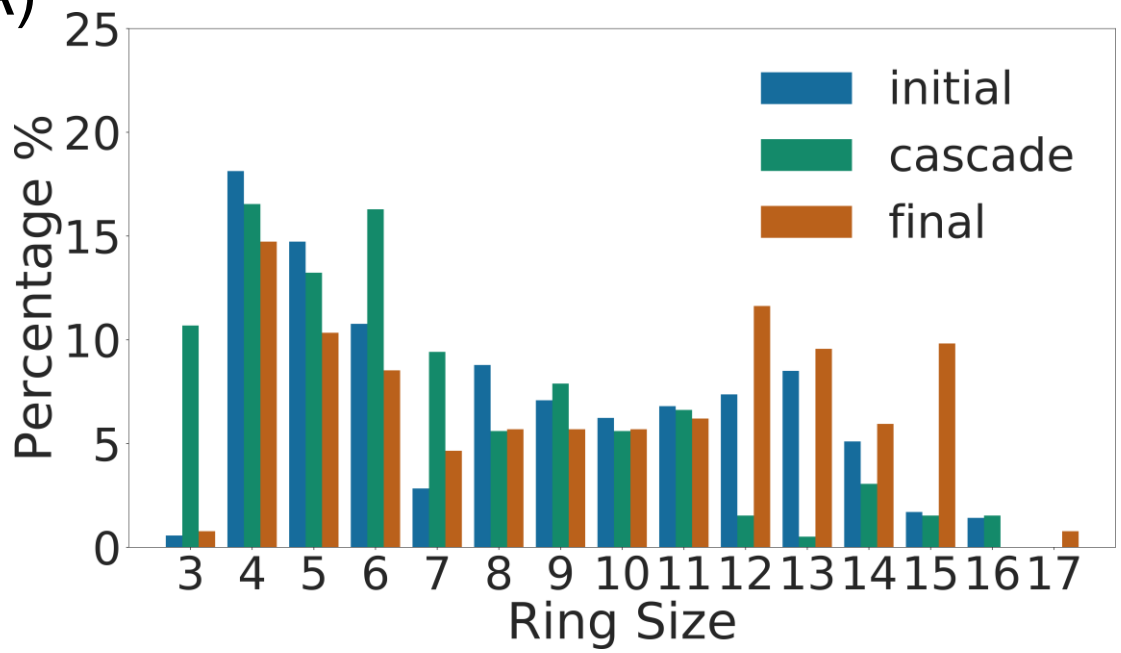
Percentage %
25
20
15
10
5
0
initial
cascade
final
3 4 5 6 7 8 9 10 11 12 13 14 15 16 17
Ring Size

(B)

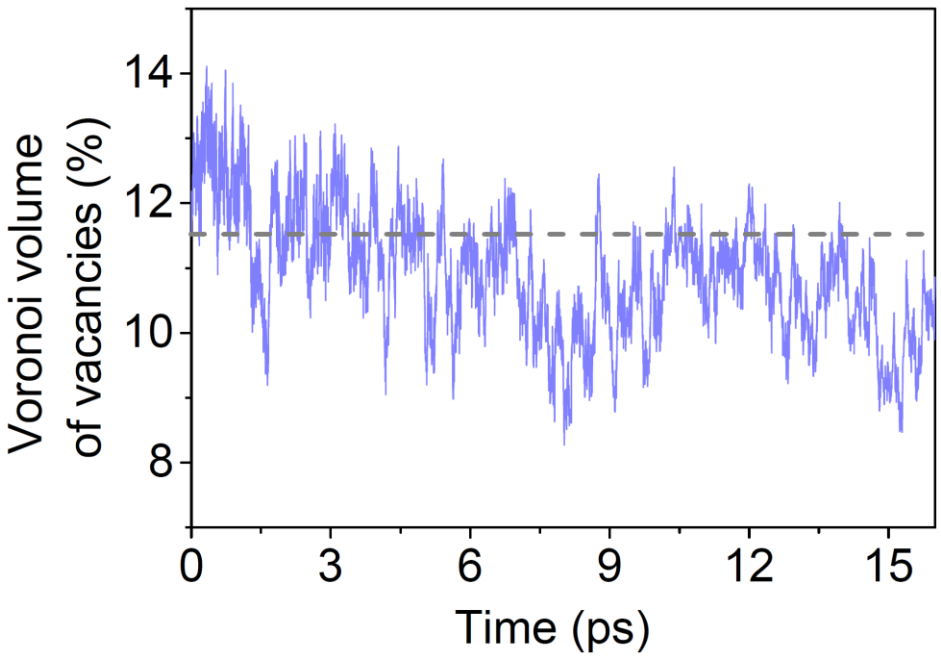
Voronoi volume of vacancies (%)
14
12
10
8
0 3 6 9 12 15
Time (ps)

(C)

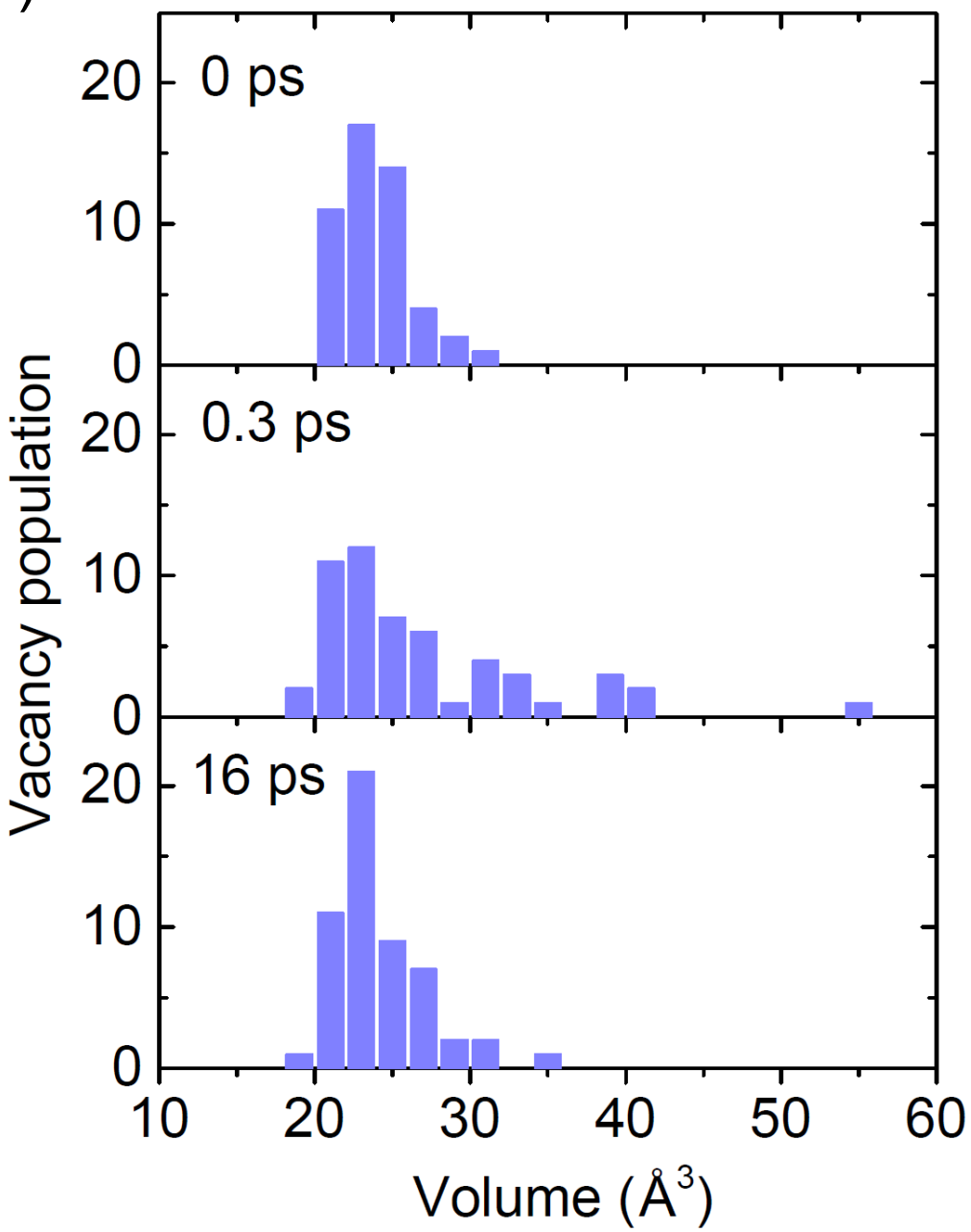

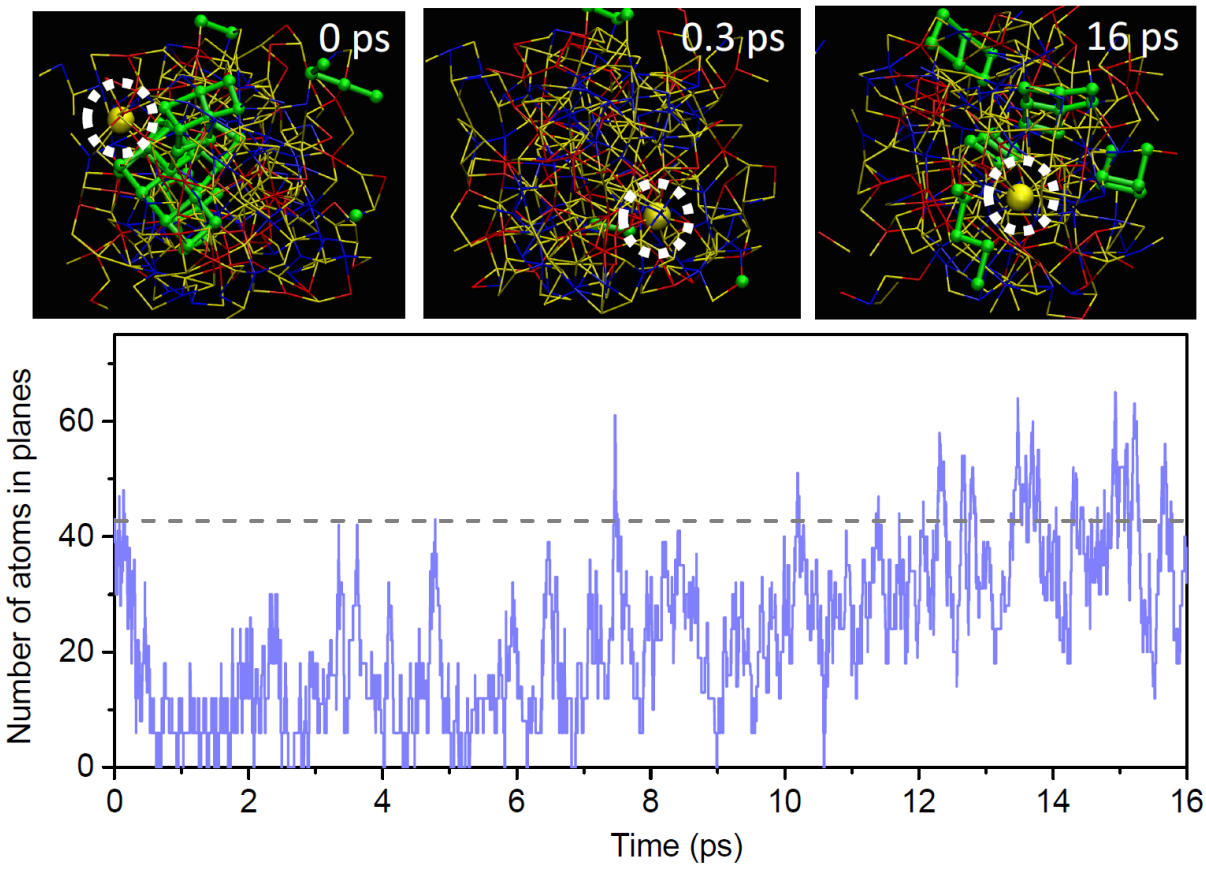
0 ps
0.3 ps
16 ps
Number of atoms in planes
0
20
40
60
0
2
4
6
8
10
12
14
16
Time (ps)

(A)

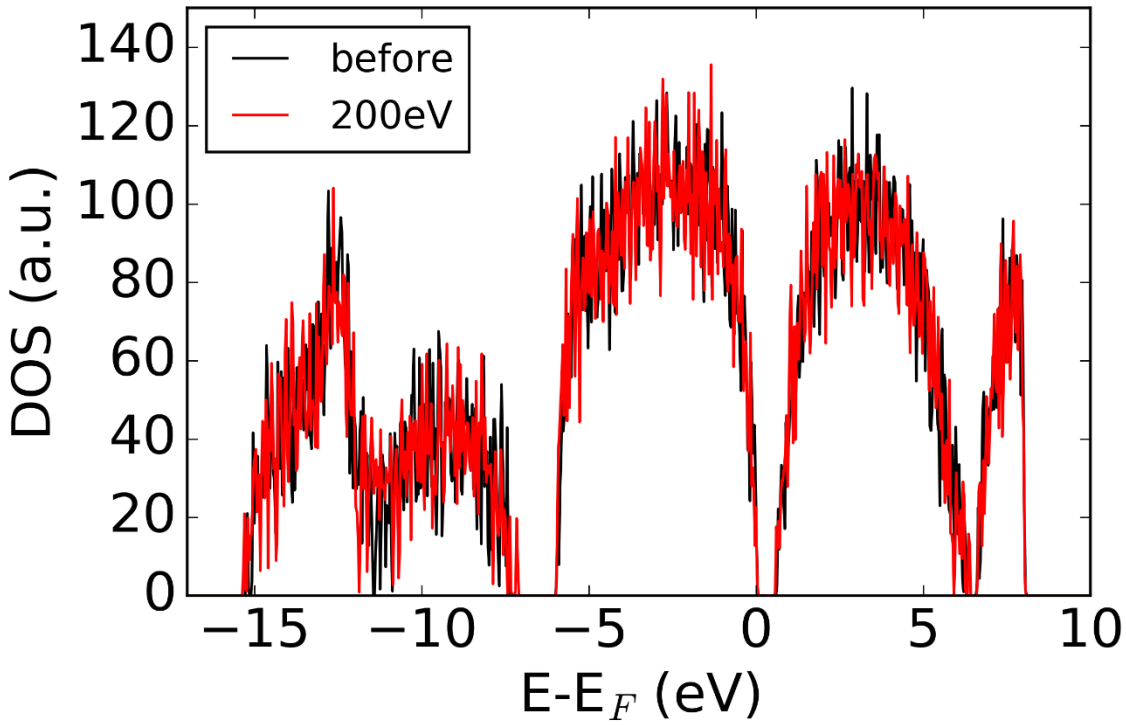
before
200eV
DOS (a.u.)
E-E$_F$ (eV)

(B)

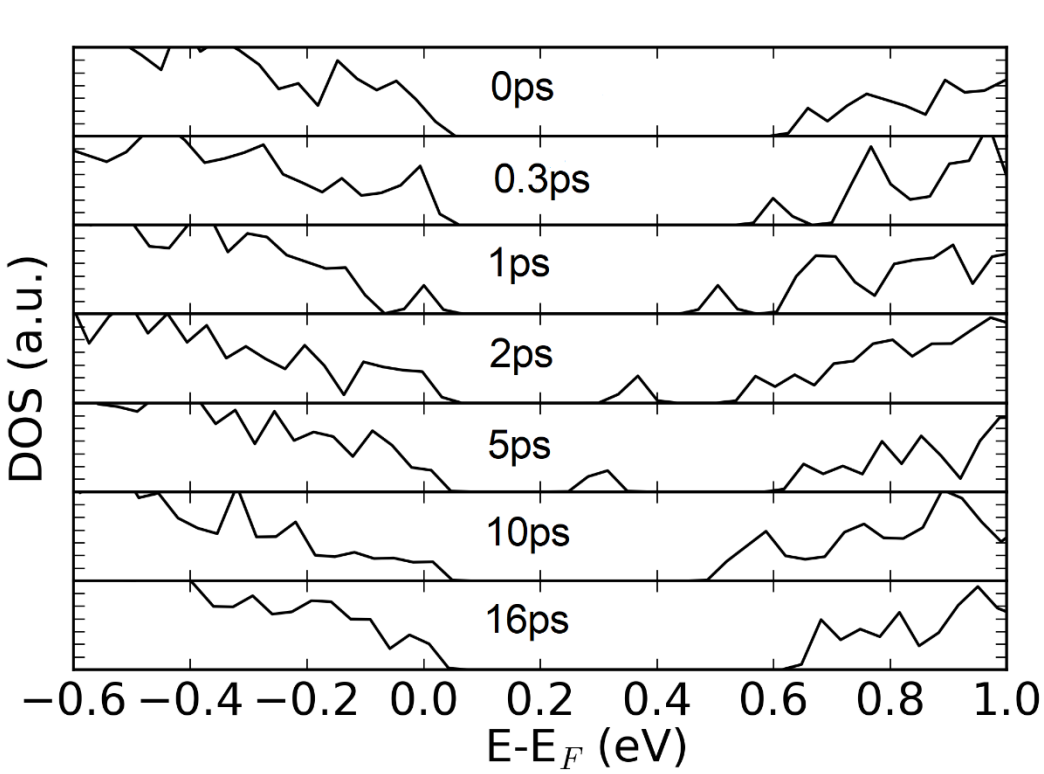
0ps
0.3ps
1ps
2ps
5ps
10ps
16ps
DOS (a.u.)
E-E$_F$ (eV)